Chinese Chemical Letters 36 (2025) 110343

Contents lists available at ScienceDirect

Chinese Chemical Letters

journal homepage: www.elsevier.com/locate/cclet

Multi-mode luminescence anti-counterfeiting and visual iron(III) ions RTP detection constructed by assembly of CDs&Eu^{3+} in porous RHO zeolite

Siyu Zong, Xiaowei Yu, Yining Yang, Xin Yang, Jiyang Li*

State Key Laboratory of Inorganic Synthesis and Preparative Chemistry, Jilin University, Changchun 130012, China

ARTICLE INFO

Article history:
Received 10 May 2024
Revised 15 July 2024
Accepted 14 August 2024
Available online 15 August 2024

Keywords:
Carbon dots
Zeolite
Host-guest assembly
Multi-mode luminescence
Phosphorescence detection
Information encryption

ABSTRACT

Carbon dots (CDs)-based composites have shown impressive performance in fields of information encryption and sensing, however, a great challenge is to simultaneously implement multi-mode luminescence and room-temperature phosphorescence (RTP) detection in single system due to the formidable synthesis. Herein, a multifunctional composite of Eu&CDs@pRHO has been designed by co-assembly strategy and prepared *via* a facile calcination and impregnation treatment. Eu&CDs@pRHO exhibits intense fluorescence (FL) and RTP coming from two individual luminous centers, Eu^{3+} in the free pores and CDs in the interrupted structure of RHO zeolite. Unique four-mode color outputs including pink (Eu^{3+}, ex. 254 nm), light violet (CDs, ex. 365 nm), blue (CDs, 254 nm off), and green (CDs, 365 nm off) could be realized, on the basis of it, a preliminary application of advanced information encoding has been demonstrated. Given the free pores of matrix and stable RTP in water of confined CDs, a visual RTP detection of Fe^{3+} ions is achieved with the detection limit as low as 9.8 μmol/L. This work has opened up a new perspective for the strategic amalgamation of luminous guests with porous zeolite to construct the advanced functional materials.

Carbon dots (CDs), as a novel zero dimensional carbon nanomaterial, have broad application prospects in sensing, anti-counterfeiting, information encryption, biological imaging and other fields due to their excellent luminescent properties [1–7]. However, bare CDs are prone to aggregation and fluorescence quenching, and their triplet states are easily quenched by oxygen and water in the environment, which limits their application to some extent. To overcome these issues and further develop advanced multiple-functional materials of CDs, various host matrix materials including organic polymers, inorganic salts, porous materials, *etc.*, are used to confine guest CDs [8–10]. Up to now, various CDs-based composites have been prepared, and their optical properties are significantly improved owing to the matrix confinement and protection, particularly in the aspect of room temperature phosphorescence (RTP) that can achieve full spectrum emissions from blue to red [11–13].

Based on the excellent fluorescence (FL) and RTP properties, CDs-based composites show great potential in optical information encryption [14,15]. Multimode luminescence can be presented in CDs-based composites due to the unique excitation-dependent FL and afterglow of CDs, as well as the integrating of additional luminescent center in the composite. By now, the CDs-containing composites with 3-mode luminescence have been developed for multi-level anti-counterfeiting. For examples, CDs@YF_3:Yb,Tm composite exhibited blue FL and green RTP of CDs, as well as upconversion luminescence of Tm^{3+} [16]. sc-CDs display blue FL, cyan RTP, and green RTP by simple regulating excitation wavelength [17]. CDs@EuAPO-5 displayed blue FL and green RTP of CDs, as well as pink FL from Eu^{3+} [18]. NOCQDs and B-CDs can exhibit blue and green afterglow with changes in excitation [19,20]. However, it is difficult to achieve multilevel luminescence than triple emission in a single composite material due to the complicated preparation method.

On the other hand, CDs and CDs-related composites have attracted great attention as the environmentally friendly fluorescent sensors for detecting various organic compounds and metal ions [21–23]. Compared to traditional FL detection, RTP detection has a higher signal-to-noise ratio and can eliminate FL interference from the background, making it a promising and transformative method in the field of luminescent sensor [24–29]. However, due to the fact that bare CDs cannot maintain stable RTP output in water, and the CDs encapsulated in the matrix cannot effectively contact the

* Corresponding author.
E-mail address: lijiyang@jlu.edu.cn (J. Li).

https://doi.org/10.1016/j.cclet.2024.110343
1001-8417/

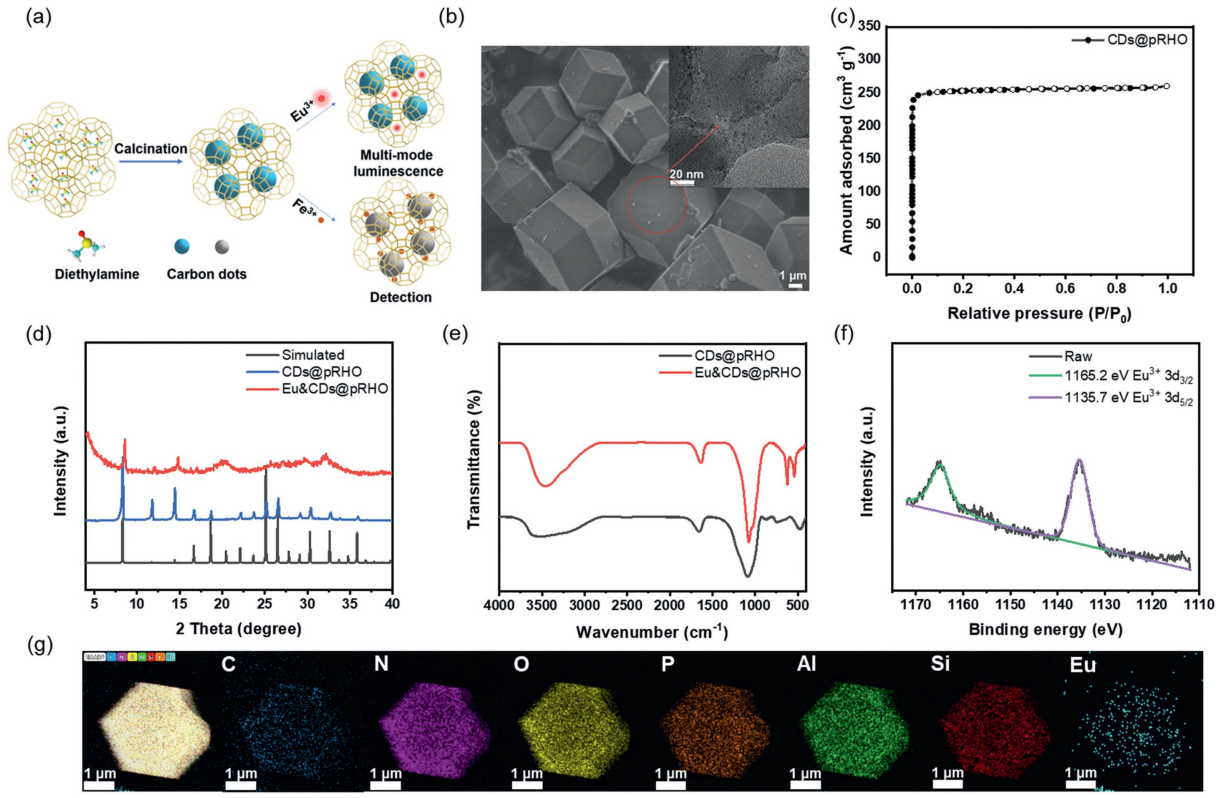

Fig. 1. (a) Schematic illustration of strategically design and application of CDs-based composite. (b) SEM and TEM (inset) images of CDs@pRHO composite. (c) N_2 adsorption-desorption isotherm of CDs@pRHO composite. (d) XRD patterns of as-made composites and simulated RHO zeolite. (d) N_2 adsorption-desorption isotherm of CDs@pRHO composite. (e) FTIR spectra of as-made composites. (f) High-resolution Eu 3d XPS spectra of Eu&CDs@pRHO and the fitting results. (g) TEM-EDS images of Eu&CDs@pRHO composite.

test substance, the research of RTP detection of CDs is greatly limited. There are only few reports on RTP detection of CDs, and the detection efficiency is far from that of FL sensors of CDs that can reach a minimum of nanomolar level.

Zeolites with unique nanoporous structures are considered an ideal matrix candidate for loading CDs and various other guest species [30–35]. The excellent thermal stability of zeolite makes it possible to prepare CDs@zeolite composite by a simple calcination, and the matrix protection of zeolite ensures the stable phosphorescence output of such composite in solid and solution. Following these considerations, in this work, a novel composite of CDs@porous RHO (CDs@pRHO) has synthesized through a simple calcination. The small pores of RHO zeolite can slow down the high temperature carbonization of occluded organic matter, exposing micropores while generating CDs in zeolite. The exposed free pores of composite not only allow CDs to effectively contact the test substance, but also can accommodate additional light sources, *e.g.*, Eu^{3+} ions, thereby achieving optical multiplexing for advanced anti-counterfeiting and iron(III) ions RTP detection.

A multifunctional CDs-based composite is constructed by the assembly of CDs and Eu^{3+} ions with zeolite matrix, as shown in Fig. 1a. The RHO zeolite with small pores (*ca.* 3.6 Å × 3.6 Å) was synthesized hydrothermally by using diethylamine (DEA) as the organic template, then a calcination treatment was adopted to remove the organic template inside the pores, meanwhile generating CDs in RHO zeolite by the decomposition of DEA. Thermogravimetry (TG) analysis shows the rapidly weight loss occurred at about 500 °C (Fig. S1 in Supporting information), therefore 500 °C was chosen as the calcination condition to prepare CDs@pRHO composite. As shown in Fig. 1b, CDs@pRHO exhibits good crystallinity and regular polyhedral morphology, and the internal CDs can be clearly observed by transmission electron microscopy (TEM). The average size of CDs in zeolite is about 1.88 nm (Fig. S2 in Supporting information). N_2 adsorption-desorption curve (Fig. 1c) proves the successful release of organic template and producing micropores in the composite. The N_2 adsorption capacity is basically consistent with the literature reported RHO-type zeolite, indicating that CDs do not occupy the microporous space of zeolite [36]. Due to the larger size of CDs than the pore size of RHO zeolite, it is inferred that CDs exist in the discontinuous structure of zeolite. Therefore, the free micropores of CDs@pRHO composite can additionally accommodate other guest molecules to construct multiple functional materials.

To achieve multi-mode luminescence of CDs@pRHO, Eu^{3+} ions were introduced into the composite by impregnation method, the formed Eu&CDs@pRHO basically maintains the crystal structure of RHO zeolite, but the crystallinity of the matrix decreases in some degree (Fig. 1d). Transmission electron microscopy-energy dispersive spectrometer (TEM-EDS) images confirm that Eu^{3+} ions have been successfully introduced into the RHO matrix. Additionally, the distribution of elements such as C and N indicates that CDs are occluded within the zeolite (Fig. 1g). The analysis of inductive coupled plasma (ICP) result (Table S1 in Supporting information) shows that the amount of Eu element in Eu&CDs@pRHO composite is 0.3 wt%, and the Si/Al ratios of RHO matrix before and after impregnation with Eu^{3+} are almost unchanged (0.43). This demonstrates that the Eu^{3+} ions do not enter the zeolite framework, which are located in the free pores of zeolite matrix [37–39]. It is noted that the appropriate calcination temperature and impregnation conditions are crucial for the synthesis of Eu&CDs@pRHO composite. A lower calcination temperature may retain more CDs, but lead to insufficient exposure of the free pores

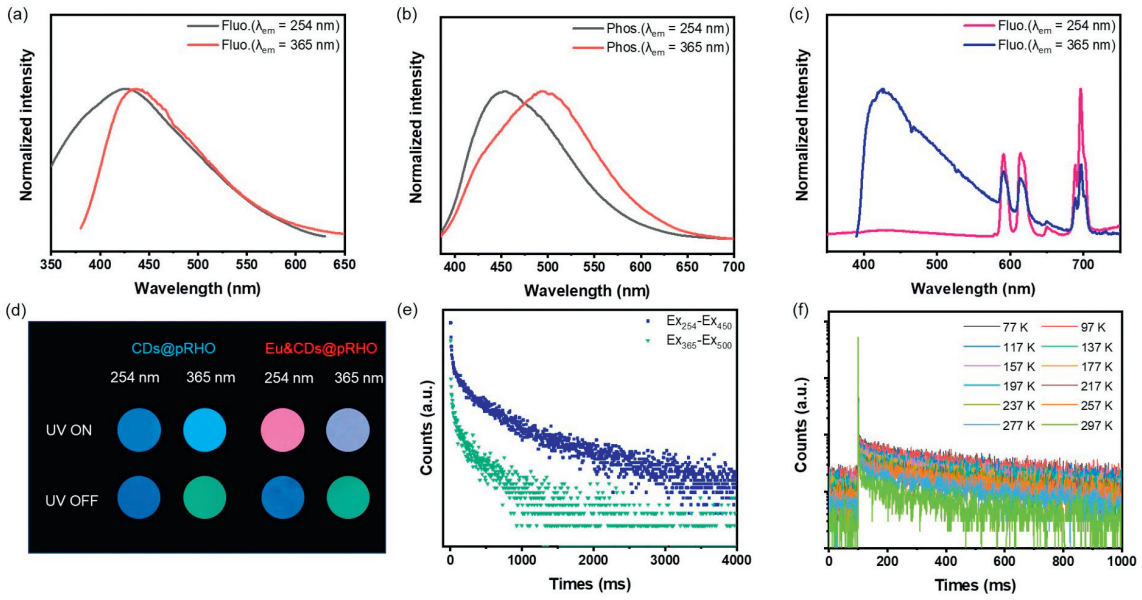

Fig. 2. The steady-state spectra of CDs@pRHO (a) and Eu&CDs@pRHO (c) excited under 254 nm and 365 nm at room temperature. (b) The delayed photoluminescence spectra of CDs@pRHO excited under 254 nm and 365 nm at room temperature (the delay time is of 1 ms). (d) Images of CDs@pRHO and Eu&CDs@pRHO with UV lamp off with time. (e) Delayed lifetimes of CDs@pRHO after 254 nm and 365 nm excitations, respectively. (f) Temperature-dependent transient photoluminescence decay of CDs@pRHO at 450 nm emission after 254 nm excitation.

of zeolite, thereby limiting the introduction of Eu^{3+} ions. On the other hand, a higher impregnation temperature and longer time may cause the collapse of the zeolite skeleton, thus affecting the overall performance of the composite.

To demonstrate the existence form of Eu^{3+} and CDs in the composite, the Fourier transform infrared spectrometry (FTIR) and X-ray photoelectron spectroscopy (XPS) analyses were characterized. As shown in Fig. 1e, the characteristic peaks of fingerprint regions at 624 cm^{-1} and 440 cm^{-1} correspond to Eu-O [40], which may be due to the coordination between Eu^{3+} in the pores and hydroxyl groups of CDs or zeolite matrix. There is no diffraction peak of Eu_2O_3 in the X-ray diffractometer (XRD) pattern of Eu&CDs@pRHO, thus the Eu-O bond does not originate from the oxide of Eu_2O_3. The peaks around 1600 cm^{-1} and 1100 cm^{-1} are assigned to the stretching vibrations of C=C and C–O/C–N bonds, respectively, which come from CDs in zeolite matrix [41,42]. In XPS survey spectrum, the peak at 1136.23 eV is characteristic for trivalent Eu 3d (Fig. S3a in Supporting information), while the peaks at 1135.7 eV and 1165.2 eV in the high-resolution XPS spectrum are the characteristic peaks of the core energy level of Eu 3d, which are Eu^{3+} $3d_{5/2}$ and Eu^{3+} $3d_{3/2}$, respectively (Fig. 1f) [43–45]. As for CDs, there are two peaks in the high-resolution C 1s XPS spectrum, C=C/C–C (284.6 eV) and C–O/C–N (286.3 eV), indicating that the CDs are composed of carbon core and nitrogen oxygen functional groups on the surface (Figs. S3b and c in Supporting information) [46]. The UV–vis absorption spectrum of isolated CDs exhibits two main absorption bands approximately at 250–300 nm and 350–400 nm, respectively, attributed to the π-π^* transition of carbon core and the n-π^* transition of surface functional groups of CDs (Fig. S4 in Supporting information) [47].

The FL properties of CDs@pRHO and Eu&CDs@pRHO were first studied. As illustrated in Fig. 2a, the FL emission of CDs@pRHO exhibits excitation dependence, which is a typical property of CDs. Under 254 nm excitation, the emission wavelength is 425 nm, which shifts to 440 nm under 365 nm excitation, correspondingly, the transition from deep-blue to light-blue can be observed with the naked eye (Fig. 2d). As for Eu&CDs@pRHO, a strong and broad emission peak at 440 nm is observed when excited by 365 nm coming from the emission of CDs (Fig. 2c). In addition, four narrow emission peaks appear at 592, 615, 653, and 699 nm, corresponding to the charge transfer from the $^5D_0$ energy level of Eu^{3+} to $^7F_1$, $^7F_2$, $^7F_3$, and $^7F_4$ [48]. When excited by 254 nm, the emission of CDs is almost invisible due to the strong emission peaks of Eu^{3+}. This corresponds to the FL excitation spectrum of Eu&CDs@pRHO (Fig. S5 in Supporting information), which is attributed to the charge transfer from O^{2-} to Eu^{3+} in Eu-O. As a result, the pink (ex. 254 nm) and light violet (ex. 365 nm) can be clearly observed with the naked eye. According to FL spectra of Eu&CDs@pRHO, it can be concluded that Eu^{3+} ions and CDs in composite emit light independently and do not affect each other, indicating that there is no interaction between Eu^{3+} ions and CDs. Therefore, the Eu-O bonds originate from the coordination between Eu^{3+} and hydroxyl groups in the zeolite framework.

The protection of zeolite matrix makes CDs@pRHO exhibit the stable visible RTP emission. Blue (450 nm) and green (500 nm) afterglow emissions could be observed after 254 nm and 365 nm radiation, respectively (Fig. 2b). This is attributed to the multiple luminescent centers of CDs in the matrix produced by the uneven calcination [20,49]. Based on the time-resolved afterglow decay curves, the RTP lifetimes of CDs@pRHO are calculated to be 340.4 ms and 572.1 ms after excitation at 365 nm and 254 nm, respectively (Fig. 2e). The temperature-dependent transient photoluminescence decay from 77 K to 297 K indicates that the proportion of delayed components decreases with increasing temperature, suggesting that the afterglow phenomenon is not affected by thermal energy, which is a characteristic of phosphorescent materials (Fig. 2f and Fig. S6 in Supporting information). As the RTP emission comes from CDs in matrix, Eu&CDs@pRHO has similar afterglow and lifetimes with that of CDs@pRHO (Figs. S7 and S8 in Supporting information). According to our previous work, the luminous lifetime of Eu^{3+} is in the microsecond range and cannot be observed with the naked eye [18]. Notably, only a small spectral overlap near 400 nm is found between the emission of CDs@pRHO and the UV–vis absorption of Eu^{3+} ions (Fig. S9 in Supporting information), which makes it difficult to achieve effective energy transfer between Eu^{3+} and CDs.

The possible luminescence mechanism of Eu&CDs@pRHO has been proposed in Fig. 3a. There are two kinds of luminous source

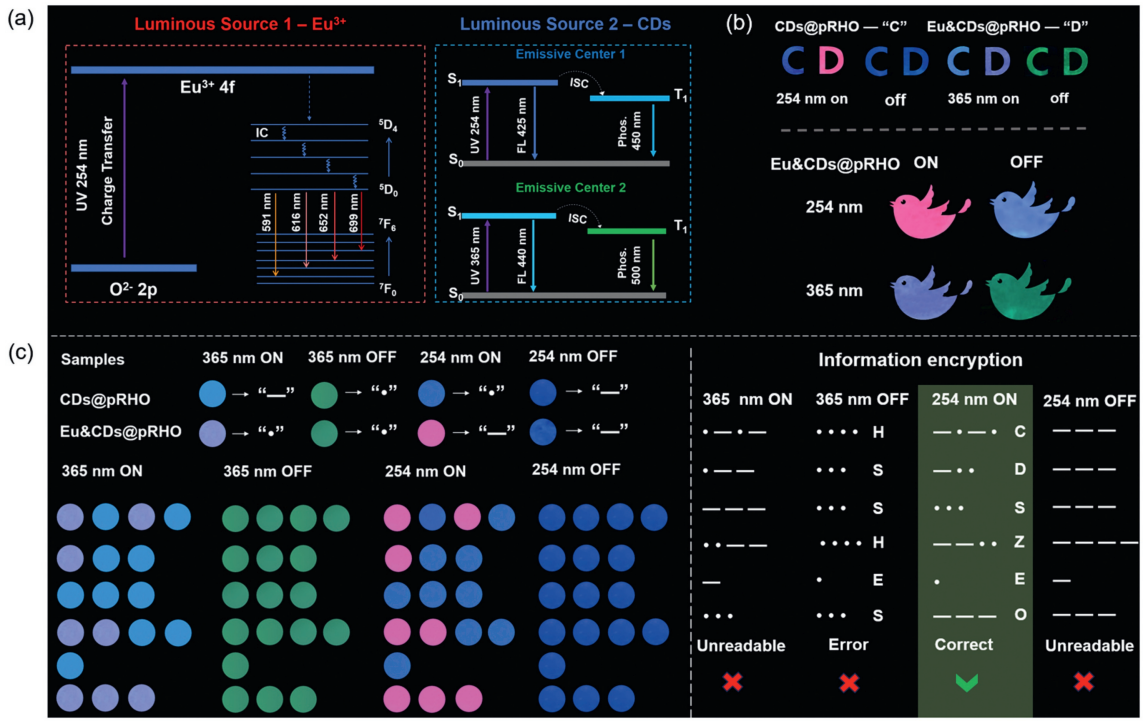

Fig. 3. (a) Proposed transformation possesses of CDs and Eu^{3+} ions in zeolite and their luminescence mechanism, respectively. (b) Four-level luminescence anti-counterfeiting of Eu&CDs@pRHO composite. (c) Demonstration of the information encoding/decoding application.

in the composite, one is Eu^{3+} in the pores of zeolite, which forms coordination bonds with -OH on the skeleton. When excited of 254 nm, the charges transfer from the 2p orbital of O^{2-} to the 4f shells of Eu^{3+}, and then transfer to the $^5D_0$ energy level through nonradiative relaxation. Then, the charges jump from $^5D_0$ energy level of Eu^{3+} to $^7F_1$, $^7F_2$, $^7F_3$, and $^7F_4$ energy level, exhibiting four emission peaks at 592 nm, 615 nm, 653 nm, and 699 nm, respectively. The other is CDs formed by the carbonization of organic components in the zeolite matrix during high-temperature calcination. Due to uneven heating under high temperature conditions, the luminescent centers of the CDs are not unique. With the alteration of excitation wavelengths, certain emission centers will dominate the RTP process, displaying different colors. As a result, under excitation at 254 nm, CDs exhibit FL emission centered at 425 nm. After removing the UV lamp, excitons transition to the T_1 state through intersystem crossing (ISC), exhibiting blue RTP emission at 450 nm. On the other hand, when excited at 365 nm, the FL peak of CDs shifts red to 440 nm, and a green RTP of 500 nm is emitted after stopping the excitation.

The unique multi-color luminescent properties of such composite have shown broad application prospects in anti-counterfeiting and information encryption. As shown in Fig. 3b, CDs@pRHO and Eu&CDs@pRHO can be drawn into different letters or patterns. Under different UV light on/off, these anti-counterfeiting signs display different color outputs. Especially, Eu&CDs@pRHO shows rare 4-mode anti-counterfeiting, which can display four color variations: pink, blue, light violet, and green. Thus, a visual information encryption system between four mode luminescent states and Morse codes has been constructed (Fig. 3c). The luminescence signals of the CDs@pRHO at 365 nm UV on and 254 nm UV on are defined as "dash (-)" and "dot (·)" in the Morse codes, respectively, while Eu&CDs@pRHO is the opposite. And the afterglow signals of the two composites (CDs@pRHO and Eu&CDs@pRHO) at 365 nm UV off and 254 nm UV off are defined as "dot (·)" and "dash (-)" in the Morse codes, respectively. According to this rule, we can encode the entire alphabet and then transcode the information to be encrypted. The constructed luminous matrix that is turned on and off under UV lamp has an interfering effect, while the correct information is hidden in the luminous matrix under 254 nm UV on. According to the encoding rules, the decoded information is displayed as "CDsZeo". Under other conditions, the luminous matrix can only decode error information and may not even be readable.

Inspired by the introducing of Eu^{3+} ions in CDs@pRHO, other metal ions can also be accommodated in the pores of composite to facilitate the detection of ions. Compared to FL, the RTP materials exhibit enormous potential for ion detection due to their long lifetimes and high signal-to-noise ratio. CDs@pRHO can maintain stable RTP output in water, making that an ideal candidate for detecting ions in solutions. As shown in Fig. 4a, CDs@pRHO exhibits optimal RTP emission under 295 nm excitation. We investigate the quenching effect of Fe^{3+} ions with concentration from 0 to 0.5 mmol/L on the RTP intensity under optimal excitation conditions by sensitivity titration. With the increase of Fe^{3+} ions, the RTP intensity of CDs@pRHO gradually decreases, and the quenching degree of RTP can exceed 80%. The limit of detection (LOD) for Fe^{3+} in the range of 0–0.5 mmol/L is 9.8 μmol/L ($3\sigma/k$) with a K_{sv} of 7.84×10^3 L/mol (Fig. 4b). There is a reasonable linear correlation between quenching efficiency and Fe^{3+} concentration (R^2=0.998) in the range of 0–0.2 mmol/L. Consequently, a visual phosphorescence detection system that can eliminate background interference has been constructed (Fig. 4c). The intense blue FL and green RTP are visible upon 365 nm excitation in the absence of Fe^{3+} ions, however, both of them are disappeared in the presence of Fe^{3+}. On the other hand, FL detection for Fe^{3+} ions were also conducted on CDs@pRHO and the isolated CDs (Figs. 4d and e, Fig. S10 in Supporting information). In the range of 0–1.5 mmol/L, the calculated LOD of CDs@pRHO and isolated CDs are 3.6 μmol/L and 35.7 μmol/L, respectively, which is not significantly different from the RTP detection values, indicating that the quenching mechanism of FL and RTP is the same. The selectivity of CDs@pRHO towards different ions was evaluated, and its RTP shows good sensing selectivity towards Fe^{3+} ions, while without significant quenching ef-

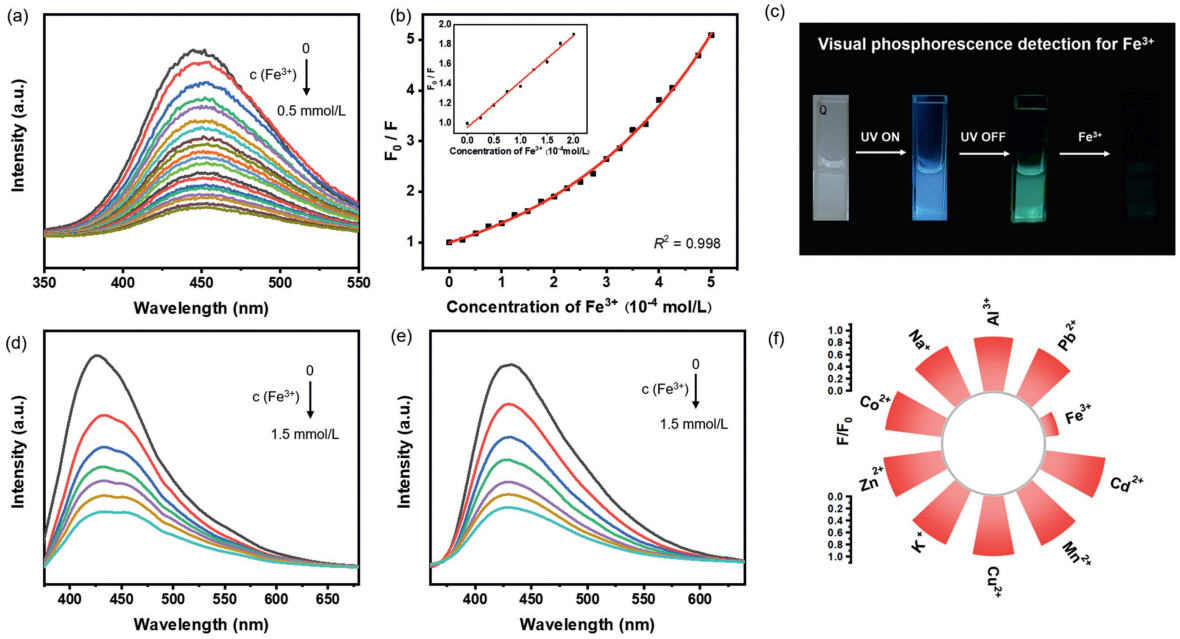

Fig. 4. (a) RTP emission spectra of CDs@pRHO with different Fe^{3+} concentrations in water (295 nm excitation). (b) Stern-Volmer plot (Inset: enlarge view of a selected area) of CDs@pRHO RTP detection for Fe^{3+}. (c) Photographs of CDs@pRHO solution in sunlight, with UV on/off, and with the addition of Fe^{3+}, respectively. (d) FL emission (350 nm excitation) spectra of CDs@pRHO with different Fe^{3+} concentrations in water. (e) FL emission (330 nm excitation) spectra of isolated CDs with different Fe^{3+} concentrations in water. (f) Normalized phosphorescent intensities of CDs@pRHO with other metal ions.

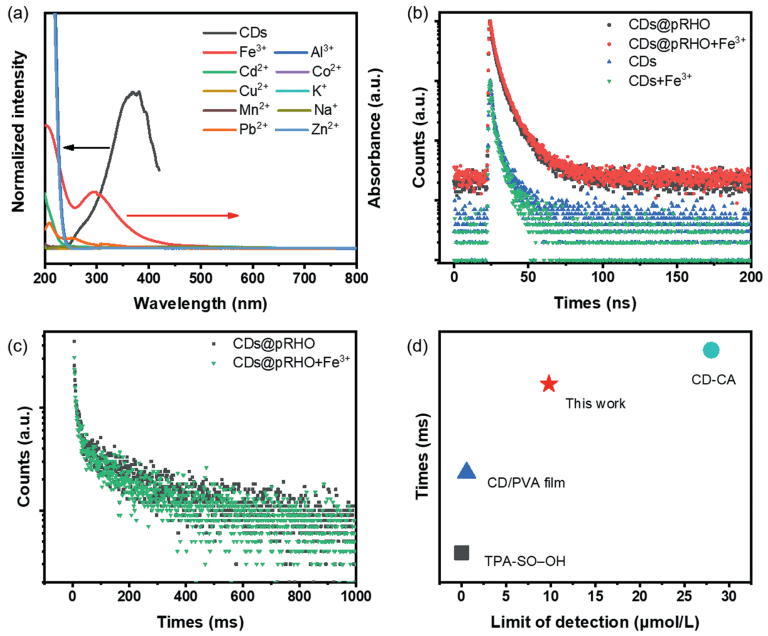

Fig. 5. (a) UV–vis spectra of various metal ions and excitation spectrum of isolated CDs. (b) FL decay curves of isolated CDs/CDs@pRHO before and after addind Fe^{3+} ions. (c) RTP decay curves of CDs@pRHO before and after addind Fe^{3+} ions. (d) The lifetimes of afterglow CDs and the detection limit of Fe^{3+} ions.

fect on other metal ions (Fig. 4f). As shown in Fig. S11 (Supporting information), when other metal ions coexist with Fe^{3+} ions, Fe^{3+} ions can still effectively quench the RTP of CDs, and the degree of quenching is almost unaffected by other metal ions.

Further exploration was conducted on the detection mechanism of CDs@pRHO to Fe^{3+} ions. As shown in Fig. 5a, the absorption spectrum of Fe^{3+} ions overlaps significantly with the excitation spectrum of CDs, while there is almost no overlap with other ions. This indicates a competitive relationship between Fe^{3+} ions and CDs in solution, leading to luminescence quenching, which is a typical feature of the internal filtration effect (IFE) [50]. Furthermore, the FL and RTP lifetimes before and after adding Fe^{3+} ions were measured (Figs. 5b and c, Tables S3 and S4 in Supporting information), which are 5.2 ns/5.4 ns (FL of CDs@pRHO), 183.6 ms/176.7 ms (RTP of CDs@pRHO) and 4.4 ns/4.0 ns (FL of isolated CDs), respectively. This means that the luminescence lifetimes of CDs@pRHO and isolated CDs remain basically the same with or without Fe^{3+} ions. Therefore, the quenching mechanism of CDs belongs to the static quenching process, which further proves that the luminescence quenching of CDs by Fe^{3+} is IFE. Finally, the performance of CDs-based materials for afterglow detection of Fe^{3+} ions were compared (Fig. 5d) [51–53]. Compared with rare reported materials, CDs@pRHO material maintains a relatively long afterglow lifetime and also having a lower detection limit, which

is attributed to protection of zeolite matrix and the unique porous characters.

In summary, a feasible strategy is presented to construct Eu&CDs@pRHO composite with 4-level luminescence and RTP detection by assembly of CDs and Eu^{3+} with RHO zeolite *via* simple calcination and impregnation. Remarkably, the porous zeolite matrix not only hosts and stables different guest luminous species, but also could adsorb metal ions and promote RTP sensing of Fe^{3+} in water. As a result, variable FL and RTP emissions could be triggered by a specific excitation wavelength (254 nm or 365 nm), displaying up to four different colors that are pink fluorescence mainly coming from Eu^{3+}, as well as light violet FL and blue/green RTP associated with CDs. In addition, CDs@pRHO exhibits excellent RTP detection performance for Fe^{3+} ions, with a detection limit of 9.8 μmol/L. The stable afterglow output in water and long lifetimes of CDs@pRHO, allowing quenching to be observed by naked eyes. In view of unique luminescent properties of Eu&CDs@pRHO and CDs@pRHO, a potential of high-level anti-counterfeiting application and visual RTP detection platform is demonstrated. This work provides a new opportunity for the development of composites that can accommodate multiple guest molecules in porous materials.

Declaration of competing interest

The authors declare that they have no known competing financial interests or personal relationships that could have appeared to influence the work reported in this paper.

CRediT authorship contribution statement

Siyu Zong: Writing – original draft, Formal analysis, Data curation, Conceptualization. **Xiaowei Yu:** Investigation, Formal analysis, Data curation. **Yining Yang:** Formal analysis, Data curation. **Xin Yang:** Formal analysis, Data curation. **Jiyang Li:** Writing – review & editing, Supervision, Software, Resources, Project administration, Conceptualization.

Acknowledgments

This work was supported by the National Natural Science Foundation of China (No. 22288101) and the 111 Project (No. B17020).

Supplementary materials

Supplementary material associated with this article can be found, in the online version, at doi:10.1016/j.cclet.2024.110343.

References

[1] X. Yang, G.I.N. Waterhouse, S. Lu, et al., Chem. Soc. Rev. 52 (2023) 8005–8058.
[2] S. Zhang, Y. Yang, Y. Zhai, et al., Chin. Chem. Lett. 34 (2023) 107652.
[3] Y. Yu, Q. Zeng, S. Tao, et al., Adv. Sci. 10 (2023) 2207621.
[4] C. Liu, X. Lin, J. Liao, et al., Chin. Chem. Lett. 35 (2024) 109598.
[5] B. Wang, G.I.N. Waterhouse, S. Lu, Trends Chem. 5 (2023) 76–87.
[6] M. Fang, B. Wang, X. Qu, et al., Chin. Chem. Lett. 35 (2024) 108423.
[7] X. Yang, X. Li, B. Wang, et al., Chin. Chem. Lett. 33 (2022) 613–625.
[8] H. Zhang, B. Wang, X. Yu, et al., Angew. Chem. Int. Ed. 59 (2020) 19390–19402.
[9] M. Shi, Q. Gao, J. Rao, et al., J. Am. Chem. Soc. 146 (2024) 1294–1304.
[10] W. Shi, R. Wang, J. Liu, et al., Angew. Chem. Int. Ed. 62 (2023) e202303063.
[11] S. Song, K. Liu, X. Mao, et al., Adv. Mater. 35 (2023) 2212286.
[12] J. Liu, Y. Luo, Z. Ran, et al., Chem. Eng. J. 474 (2023) 145597.
[13] Y. Ding, X. Wang, M. Tang, et al., Adv. Sci. 9 (2022) 2103833.
[14] X. Wei, J. Yang, L. Hu, et al., J. Mater. Chem. C 9 (2021) 4425–4443.
[15] J. Li, X. Gong, Small 18 (2022) 2205099.
[16] P. Liang, Y. Zheng, F. Liu, et al., JACS Au 3 (2023) 2291–2298.
[17] Q. Li, S. Meng, Y. Li, et al., Carbon 195 (2022) 191–198.
[18] X. Yu, K. Liu, H. Zhang, et al., Small 17 (2021) 2103374.
[19] L. Yang, Q. Zhang, Y. Ma, et al., Chem. Eng. J. 490 (2024) 151679.
[20] T. Li, C. Wu, M. Yang, et al., Langmuir 38 (2022) 2287–2293.
[21] Z. Li, J. Hou, S. Wang, et al., Coordin. Chem. Rev. 469 (2022) 214695.
[22] D. Su, H. Li, X. Yan, et al., Trends Anal. Chem. 134 (2021) 116126.
[23] Y. Dong, J. Cai, X. You, et al., Analyst 140 (2015) 7468–7486.
[24] Z. An, C. Zheng, Y. Tao, et al., Nat. Mater. 14 (2015) 685–690.
[25] X. Yang, D. Yan, Chem. Sci. 7 (2016) 4519–4526.
[26] N. Wang, T. Zhou, J. Wang, et al., Analyst 135 (2010) 2386–2393.
[27] Y. Zhou, W. Qin, C. Du, et al., Angew. Chem. Int. Ed. 58 (2019) 12102–12106.
[28] Q. Feng, Z. Xie, M. Zheng, et al., Sens. Actuators B: Chem. 351 (2022) 130976.
[29] Q. Wang, Q. Tan, S. Zhao, et al., Chem. Eng. J. 470 (2023) 144061.
[30] J. Liu, N. Wang, Y. Yu, et al., Sci. Adv. 3 (2017) e1603171.
[31] X. Yu, K. Liu, B. Wang, et al., Adv. Mater. 35 (2023) 2208735.
[32] H. Zhang, K. Liu, J. Liu, et al., CCS Chem. 2 (2020) 118–127.
[33] B. Wang, Y. Yu, H. Zhang, et al., Angew. Chem. Int. Ed. 58 (2019) 18443–18448.
[34] X. Yu, K. Liu, H. Zhang, et al., CCS Chem. 3 (2021) 252–264.
[35] B. Wang, S. Zong, J. Li, Chem. J. Chin. Univ. 42 (2021) 299–310.
[36] X. Wang, N. Yan, M. Xie, et al., Chem. Sci. 12 (2021) 8803–8810.
[37] L. Wang, C. Lin, I. Boldog, et al., Angew. Chem. Int. Ed. 63 (2024) e202317435.
[38] J. Qian, W. Zhang, X. Yang, et al., Sep. Purif. 309 (2023) 123078.
[39] K.S. Kencana, J.G. Min, K.C. Kemp, et al., Sep. Purif. 282 (2022) 120027.
[40] L. Lin, X. Song, Y. Chen, et al., Anal. Chim. Acta 891 (2015) 261–268.
[41] Y. Zhang, M. Li, S. Lu, Small 19 (2022) 2206080.
[42] H. Ding, S. Yu, J. Wei, et al., ACS Nano 10 (2016) 484–491.
[43] J. Sun, Z. Jia, E. Damiano, et al., CrystEngComm 20 (2018) 6741–6751.
[44] D. Kavyashree, R.A. Kumari, H. Nagabhushana, et al., J. Lumin. 167 (2015) 91–100.
[45] J. Yang, X. Li, J. Lang, et al., Mater. Sci. Semicond. Process. 14 (2011) 247–252.
[46] B. Wang, Z. Wei, L. Sui, et al., Light Sci. Appl. 11 (2022) 172.
[47] X. Yang, L. Sui, B. Wang, et al., Sci. China Chem. 64 (2021) 1547–1553.
[48] A. Balamurugan, M.L.P. Reddy, M. Jayakannan, J. Mater. Chem. A 1 (2013) 2256–2266.
[49] S. Zong, B. Wang, X. Yin, Nano Res. 15 (2022) 9454–9460.
[50] X. Mi, D. Sheng, Y. Yu, et al., ACS Appl. Mater. Interfaces 11 (2019) 7914–7926.
[51] X. Wu, C. Ma, J. Liu, et al., ACS Sustain. Chem. Eng. 7 (2019) 18801–18809.
[52] Q. Li, M. Zhou, M. Yang, et al., Nat. Commun. 9 (2018) 734.
[53] J. Yu, S. Qiu, K. Zhang, et al., J. Mol. Struct. 1251 (2022) 132074.